Monthly Notices
of the
ROYAL ASTRONOMICAL SOCIETY

MNRAS **469,** 612–620 (2017)
Advance Access publication 2017 April 11

doi:10.1093/mnras/stx892

State-to-state chemistry and rotational excitation of CH^+ in photon-dominated regions

A. Faure,[1⋆] P. Halvick,[2⋆] T. Stoecklin,[2] P. Honvault,[3] M. D. Epée Epée,[4] J. Zs. Mezei,[5,6,7,8] O. Motapon,[4,9] I. F. Schneider,[5,7⋆] J. Tennyson,[10] O. Roncero,[11] N. Bulut[12] and A. Zanchet[11]

[1]*Université Grenoble Alpes, CNRS, IPAG, F-38000 Grenoble, France*
[2]*Université Bordeaux, CNRS, ISM, F-33400 Talence, France*
[3]*Université Bourgogne Franche-Comté, Laboratoire ICB, F-21078 Dijon, France*
[4]*UFD Mathématiques, Informatique Appliquée et Physique Fondamentale, University of Douala, PO Box 24157, Douala, Cameroon*
[5]*Université Normandie, CNRS, LOMC, F-76058 Le Havre, France*
[6]*LSPM, Univ. Paris 13, 99 avenue Jean-Baptiste Clément, F-93430 Villetaneuse, France*
[7]*Université Paris-Sud, CNRS, Laboratoire Aimé Cotton, F-91405 Orsay, France*
[8]*Institute of Nuclear Research of the Hungarian Academy of Sciences, PO Box 51, Debrecen H-4001, Hungary*
[9]*University of Maroua, Faculty of Science, PO Box 814 Maroua, Cameroon*
[10]*Department of Physics and Astronomy, University College, London, Gower St., London WC1E 6BT, UK*
[11]*Instituto de Física Fundamental, CSIC, C/Serrano, 123, E-28006 Madrid, Spain*
[12]*Department of Physics, Firat University, 23169 Elazığ, Turkey*

Accepted 2017 April 7. Received 2017 April 6; in original form 2017 February 10

ABSTRACT

We present a detailed theoretical study of the rotational excitation of CH^+ due to reactive and non-reactive collisions involving $C^+(^2P)$, H_2, CH^+, H and free electrons. Specifically, the formation of CH^+ proceeds through the reaction between $C^+(^2P)$ and $H_2(\nu_{H_2} = 1, 2)$, while the collisional (de)excitation and destruction of CH^+ is due to collisions with hydrogen atoms and free electrons. State-to-state and initial-state-specific rate coefficients are computed in the kinetic temperature range 10–3000 K for the inelastic, exchange, abstraction and dissociative recombination processes using accurate potential energy surfaces and the best scattering methods. Good agreement, within a factor of 2, is found between the experimental and theoretical thermal rate coefficients, except for the reaction of CH^+ with H atoms at kinetic temperatures below 50 K. The full set of collisional and chemical data are then implemented in a radiative transfer model. Our non-LTE calculations confirm that the formation pumping due to vibrationally excited H_2 has a substantial effect on the excitation of CH^+ in photon-dominated regions. In addition, we are able to reproduce, within error bars, the far-infrared observations of CH^+ towards the Orion Bar and the planetary nebula NGC 7027. Our results further suggest that the population of $\nu_{H_2} = 2$ might be significant in the photon-dominated region of NGC 7027.

Key words: astrochemistry – line: formation – molecular data – molecular processes – radiative transfer – ISM: molecules.

1 INTRODUCTION

The methylidyne ion CH^+ was the first molecular ion to be identified from its optical absorption spectra in the diffuse interstellar medium (ISM; Douglas & Herzberg 1941). Since then, CH^+ absorption has been observed towards many background stars, demonstrating the ubiquity of this simple carbon hydride in the diffuse ISM. The mechanism by which it forms has remained however elusive. Theoretical models have been indeed unable to reproduce the large observed abundance of CH^+ in diffuse clouds, $[CH^+]/[H] \sim 8 \times 10^{-9}$ (see e.g. Godard & Cernicharo 2013, and references therein).

It was for a long time assumed that CH^+ is primarily formed by the reaction

$$C^+ + H_2 \rightarrow CH^+ + H. \quad (1)$$

⋆ E-mail: alexandre.faure@univ-grenoble-alpes.fr (AF); p.halvick@ism.u-bordeaux1.fr (PH); ioan.schneider@univ-lehavre.fr (IFS)

This reaction is barrierless but endothermic by 0.398 eV (4620 K; Hierl, Morris & Viggiano 1997), which is much higher than the kinetic temperatures in ordinary diffuse clouds ($T_k < 100$ K). As a result, non-equilibrium chemistry is necessary to explain the large column densities ($\geq 10^{13}$ cm^{-2}) of CH^+ observed in the diffuse ISM. The invoked gas heating mechanisms proposed to accelerate reaction (1) include C-type and magnetohydrodynamic shocks, Alfvèn waves, turbulent mixing and turbulent dissipation. A recent discussion of these different scenarios in the framework of UV-dominated and turbulence-dominated chemistries can be found in Godard, Falgarone & Pineau des Forêts (2014).

The vast majority of the observed CH^+ absorptions arise from the ground rotational level $j = 0$. The first excited level $j = 1$ lies 40.1 K above the ground state, and it is not sufficiently populated at the typical density of diffuse clouds where CH^+ abounds ($n_H \lesssim 10^2$ cm^{-3}). The critical density of the $j = 1 \rightarrow 0$ transition is indeed large, $n_{cr} \sim 4 \times 10^6$ cm^{-3}. Rotationally excited levels of CH^+ can be significantly populated in the diffuse ISM only in the presence of warm dust emission (Oka et al. 2013).

Emission lines from CH^+ are less commonly observed but they have been detected in the visible towards the red rectangle (e.g. Bakker et al. 1997) and in the far-infrared towards several sources: the planetary nebula NGC 7027 (Cernicharo et al. 1997), the Orion Bar (Nagy et al. 2013; Parikka et al. 2017), the Orion BN/KL complex (Morris et al. 2016), the massive star-forming region DR21 (Falgarone et al. 2010), the infrared galaxy Markarian 231 (van der Werf et al. 2010) and the disc around the Herbig Be star HD 100546 (Thi et al. 2011). The far-infrared lines arise from pure rotational transitions and they were detected thanks to the *ISO* and *Herschel* space observatories. The largest number of rotational lines was identified in NGC 7027 and in the Orion Bar, which are two prototypical photon-dominated regions (PDRs). In these two sources, the rotational series $j \rightarrow j - 1$ was observed from $j = 1 \rightarrow 0$ at 835.137 GHz up to $j = 6 \rightarrow 5$ at 4976.201 GHz. In such regions, the dense gas ($n_H > 10^4$ cm^{-3}) is illuminated by a strong far-ultraviolet (FUV) radiation field, and a reservoir of H_2 ro-vibrationally excited by FUV fluorescence can provide an alternative route to overcome the endothermicity of reaction (1) (Sternberg & Dalgarno 1995; Agúndez et al. 2010). This was evidenced recently in the Orion Bar where a good correlation between CH^+ and vibrationally excited H_2 was observed by Parikka et al. (2017).

Indeed, it has been shown both experimentally and theoretically that the internal (rotational or vibrational) excitation of H_2 can help to reduce or even offset the endothermicity of reaction (1). The rotational and vibrational energies were found to be as effective as the translational energy in promoting the reaction (Gerlich, Disch & Scherbarth 1987; Hierl et al. 1997; Zanchet et al. 2013; Herráez-Aguilar et al. 2014). As a result, the experimental rate coefficient derived by Hierl et al. (1997) for the reaction of C^+ with $H_2(v_{H_2} = 1)$ between 800 and 1300 K is in the range (1–2) $\times 10^{-9}$ cm^3 s^{-1}, in good agreement with the Langevin limit (1.6×10^{-9} cm^3 s^{-1}). This value represents an enhancement of about 3 orders of magnitude with respect to the rate coefficient of ground-state $H_2(v_{H_2} = 0)$. This finding was confirmed theoretically by two recent independent studies (Zanchet et al. 2013; Herráez-Aguilar et al. 2014). These studies were also able to derive state-to-state rate coefficients and, in particular, Zanchet et al. (2013) have provided the first rotationally resolved rate coefficients.

State-resolved rates for the production and loss of CH^+ are crucial because the rotational excitation of CH^+ is governed by the competition between the radiative processes and the j-dependent formation, destruction and collisional excitation processes. Indeed, inelastic collisions with the dominant species, i.e. hydrogen atoms, free electrons and hydrogen molecules, are not faster than the reactive processes. Thus, in contrast to non-reactive molecules such as CO, inelastic collisions can never fully equilibrate the rotational populations of CH^+. The CH^+ emission spectrum is therefore expected to retain some memory of the j-dependent formation process, as discussed in Black (1998). As a result, when solving the coupled equations of statistical equilibrium and radiative transfer, it is necessary to include state-resolved formation and destruction rates in addition to the usual radiative and inelastic rates. Strong deviations of the level populations from local thermodynamic equilibrium (LTE) are expected in these conditions.

Non-LTE calculations including formation and destruction rates were recently performed to model the CH^+ emissions observed towards NGC 7027, the Orion Bar and Orion BN/KL (Godard & Cernicharo 2013; Nagy et al. 2013; Zanchet et al. 2013; Morris et al. 2016). The most complete model is that of Godard & Cernicharo (2013), which includes the radiative pumping of CH^+ vibrational and electronic states by infrared, optical and UV photons. In all these studies, inelastic data were taken from the state-to-state calculations of Hammami, Owono Owono & Stäuber (2009) and Turpin, Stoecklin & Voronin (2010) on CH^+–He and those of Lim, Rabadán & Tennyson (1999) on CH^+–electron, and they were complemented by extrapolations. For the destruction by reactions with H, electrons and H_2, generic rates independent of j were assumed, except for $CH^+ + H$ in Godard & Cernicharo (2013) where the initial-state-specific rate coefficients extracted by Plasil et al. (2011) for $j = 0$, 1, 2 at $T_k \leq 60$ K were used. For the formation by the reaction of C^+ with H_2, the theoretical data of Zanchet et al. (2013) were employed in the most recent studies (Zanchet et al. 2013; Morris et al. 2016), while in the previous models of Godard & Cernicharo (2013) and Nagy et al. (2013), the formation rates were expressed as a Boltzmann distribution at an effective formation temperature. The major result of these studies is that in warm and dense PDR conditions, the 'formation' or 'chemical' pumping via the reaction $C^+ + H_2(v_{H_2} = 1)$ is the dominant source of the rotational excitation of $CH^+(j > 1)$. The use of initial-state-specific formation rates (instead of a Boltzmann distribution) was also found to have a substantial impact on the distribution of the highest CH^+ levels ($j \geq 4$) (Zanchet et al. 2013). Incidentally, the density in the PDR can be 1 to 2 orders of magnitude below the values inferred from traditional excitation models (Godard & Cernicharo 2013). All the models published so far were however hampered by the lack of initial-state-specific rate coefficients for the destruction of CH^+ at $T_k > 60$ K. In addition, inelastic data for $CH^+ + H$ and $CH^+ + H_2$ were simply scaled from those of $CH^+ + He$, which is questionable since collisions with H and H_2 are reactive.

Here, we provide the first comprehensive set of theoretical state-to-state rate coefficients for the inelastic and reactive collisions of CH^+ with hydrogen atoms and free electrons in the temperature range 10–3000 K. This data is computed from state-of-the-art theoretical methods using the most accurate interaction potentials. Theoretical approaches include the time-independent quantum mechanical (TIQM) method, quasi-classical trajectory (QCT) calculations, the R-matrix adiabatic nuclei approach and the multichannel quantum defect theory (MQDT). In addition, new quantum time-dependent (wave-packet) calculations are performed for the formation reaction (1) to extend the data of Zanchet et al. (2013). In the next section, the inelastic and reactive rate coefficients are described with a brief description of the different calculations. In Section 3, these rate coefficients are employed to model the CH^+ emission spectrum for typical PDR physical conditions. Our non-LTE model

is applied, in particular, to reproduce the CH^+ line fluxes observed towards the Orion Bar and the planetary nebula NGC 7027. General conclusions are drawn in Section 4.

2 INELASTIC AND REACTIVE RATE COEFFICIENTS

2.1 Formation via $C^+ + H_2$

The calculations presented in this section are an extension of the work of Zanchet et al. (2013). In those calculations, the time-dependent wave-packet (TDWP) method was combined with the potential energy surface (PES) developed by Stoecklin & Halvick (2005) for the electronic ground state of CH_2^+. Cross-sections and rate coefficients were determined for the reaction of $C^+(^2P)$ with H_2 in the ground-state ($v_{H_2} = 0$, $j_{H_2} = 0$) and in the first vibrationally excited state ($v_{H_2} = 1$, $j_{H_2} = 0, 1$) for temperatures in the range 10–5000 K. In the dynamical calculations, only one adiabatic electronic state was thus considered, neglecting spin-orbit couplings. In order to take them into account, it was assumed that the cross-sections for the two $C^+(^2P_{1/2})$ states correspond to those calculated in the adiabatic approximation, while the four $C^+(^2P_{3/2})$ states do not contribute to the reaction. The final reaction cross-sections were obtained by averaging over all spin-orbit states, considering the proper electronic partition function using the experimental spin-orbit splittings. The reaction cross-sections for $v_{H_2} = 0$ were found in good agreement with the experimental results of Gerlich et al. (1987), while the rate coefficients for $v_{H_2} = 1$ were shown to be a factor of ∼3 smaller than those derived by Hierl et al. (1997). A very similar result was obtained by Herráez-Aguilar et al. (2014) using a different PES and a different methodology (QCT calculations). Part of the disagreement between theory and experiment was attributed to the contribution of $v_{H_2} > 1$ (Zanchet et al. 2013) and to the effect of rotational excitation (Herráez-Aguilar et al. 2014) neglected in the experimental derivation. Full details on the TDWP calculations can be found in Zanchet et al. (2013).

In this work, the calculations of Zanchet et al. (2013) were extended to the second vibrationally excited state of $H_2(v_{H_2} = 2, j_{H_2} = 0)$. As we will see below, the population of $v_{H_2} = 2$ can be significant in highly FUV illuminated regions. It should be noted that while the rotational excitation of H_2 is crucial in $v_{H_2} = 0$ (because reaction (1) is endothermic for $j_{H_2} \leq 7$), it has only a modest impact in vibrationally excited levels $v_{H_2} \geq 1$ for which collisions leading to $CH^+(v = 0)$ display no threshold (Zanchet et al. 2013; Herráez-Aguilar et al. 2014). This is illustrated in Fig. 1, where we have plotted the rotational distribution of the nascent $CH^+(v = 0, j)$ product from the three reactions C^++para-$H_2(v_{H_2} = 1, j_{H_2} = 0)$, C^++ortho-$H_2(v_{H_2} = 1, j_{H_2} = 1)$ and C^++para-$H_2(v_{H_2} = 2, j_{H_2} = 0)$ at a kinetic temperature $T_k = 500$ K. We can first observe that the rotational state of $H_2(v_{H_2} = 1)$ (i.e. para or ortho ground-state) has a negligible influence on the CH^+ distribution, as expected. We also observe that the probability distributions for $v_{H_2} = 1$ and $v_{H_2} = 2$ peak at $j \sim 6$ and $j \sim 10$, respectively. These distributions do not follow Maxwell-Boltzmann functions but they have, however, a resemblance to Maxwellian distributions at $T_f = 1000$ and 5000 K, respectively. As the reaction enthalpy is ∼−1500 K for $H_2(v_{H_2} = 1, j_{H_2} = 1)$ and ∼−7000 K for $H_2(v_{H_2} = 2, j_{H_2} = 0)$, this suggests that about two-third of the exothermicity of the reaction is transferred to CH^+ rotation. Thus, although approximate and confusing, the concept of 'formation temperature' is not irrelevant. We note also that the effect of kinetic temperature is moderate in the range $T_k = 10$–5000 K: The distribution broadens with increasing temperature but the distribution peak is not shifted.

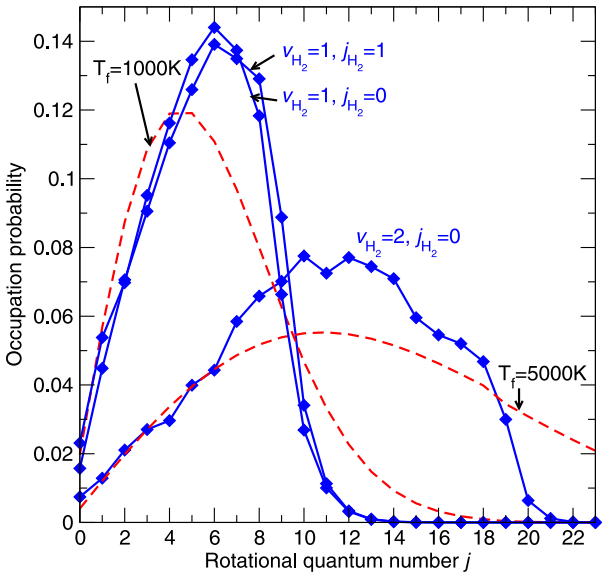

Figure 1. Occupation probability of the nascent $CH^+(v = 0, j)$ product from the reaction of C^+ with $H_2(v_{H_2} = 1, j_{H_2} = 1)$, $H_2(v_{H_2} = 1, j_{H_2} = 0)$ and $H_2(v_{H_2} = 2, j_{H_2} = 0)$ at kinetic temperature $T_k = 500$ K. The Boltzmann distributions at formation temperatures $T_f = 1000$ and 5000 K are plotted as dashed lines.

2.2 Excitation and destruction by hydrogen atoms

The calculations presented in this section are an extension of the work of Werfelli et al. (2015). In those calculations, the TIQM code ABC (Skouteris, Castillo & Manolopoulos 2000) was combined with a new full-dimensional PES for the ground electronic state of CH_2^+. The ABC code was also checked for the first time against an accurate quantum method in the case of a complex forming reaction with a deep potential well. Cross-sections and rate coefficients were determined for $CH^+(j = 0$–$7)$ and kinetic temperatures in the range 5–800 K. The thermal rate coefficients (i.e. averaged over the Boltzmann rotational distributions) were found in good agreement with the experimental data in the range 50–800 K. At lower temperatures, however, the steep fall-off observed experimentally by Plasil et al. (2011) was not reproduced by the calculations of Werfelli et al. (2015), in contrast to other recent theoretical works based on different PESs (Warmbier & Schneider 2011; Grozdanov & McCarroll 2013; Bovino, Grassi & Gianturco 2015; Li, Zhang & Han 2015). However, the analysis by Werfelli et al. (2015) has shown that those PESs have incorrect long-range behaviour and that the seemingly good agreement with the low-temperature data is fortuitous. Full details on the PES and the TIQM calculations can be found in Werfelli et al. (2015).

In this work, the calculations of Werfelli et al. (2015) were extended to $CH^+(j = 8$–$13)$ and kinetic temperatures up to $T_k = 3000$ K. Levels higher than $j = 13$ are not considered because they lie above the first vibrational threshold of CH^+ (which opens at ∼3700 K). Since TIQM calculations are computationally highly expensive for $CH^+ + H$, we resorted here to QCT calculations using the same PES as Werfelli et al. (2015). The QCT calculations were performed for 29 values of the collision energy E_c distributed in the range 1–1600 meV, thus allowing us to calculate the rate coefficients in the range 10–3000 K. Batches of 50 000

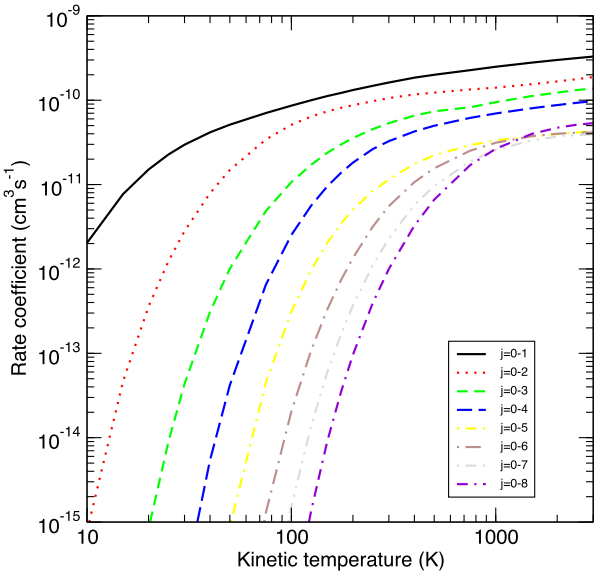

Figure 2. Rate coefficients for rotational excitation of CH$^+$ out of the ground state $j = 0$ by H as functions of the kinetic temperature. These data include both inelastic and exchange channels (see text).

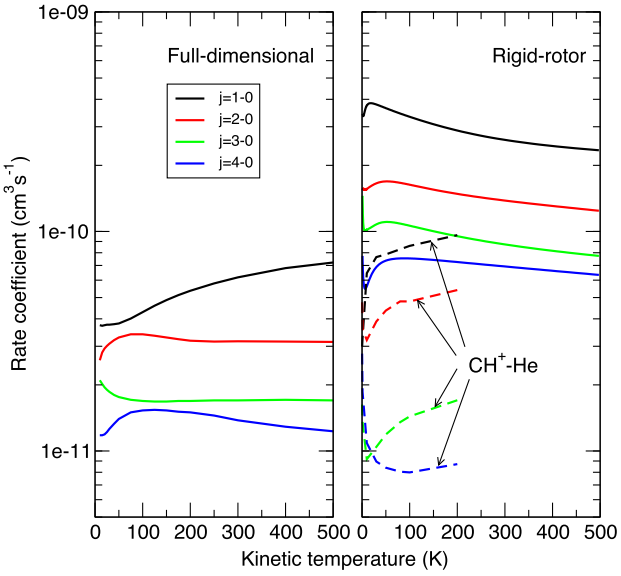

Figure 3. Rate coefficients for rotational de-excitation of CH$^+$ ($j \rightarrow 0$) by H as functions of the kinetic temperature. Full-dimensional and rigid-rotor calculations are presented in the left- and right-hand panels, respectively. The dashed lines in the right-hand panel give the results of Turpin et al. (2010) for CH$^+$+He.

trajectories were computed for each value of E_c and for each initial ro-vibrational state (v, j) of CH$^+$, with $v = 0$ and $0 \leq j \leq 13$. For each batch, the maximum impact parameter was adapted to the inelastic collisions. The zero-point energy leakage is a well-known shortcoming of QCT calculations, and it is even more pronounced as the number of open ro-vibrational levels decreases. This failure can be corrected with the help of the Gaussian binning (GB) procedure (Bonnet 2013). However, in the case of inelastic processes, the vibrationally adiabatic trajectories give large contributions that overly dominate the GB probabilities (Bonnet 2013). Therefore, we treated the vibrationally adiabatic trajectories with the standard binning procedure, and use the GB procedure for the remaining trajectories. Finally, the QCT rate coefficients were scaled in order to provide an extension up to 3000 K of the quantum rate coefficients previously calculated below 800 K and for $0 \leq j \leq 7$. For $8 \leq j \leq 13$, an average scaling factor was applied.

In Fig. 2, the rate coefficients for the sum of the inelastic (non-reactive) and exchange processes CH$^+$($j = 0$) + H $\rightarrow$ CH$^+$(j')+H are plotted as functions of the kinetic temperature for $j' = 1$–8. We observe a strong increase of the rate coefficients with increasing temperature that mainly reflects the excitation thresholds of the different transitions (e.g. $0 \rightarrow 1$ opens at 40 K). As a result, the transition with $\Delta j = 1$ is largely favoured at low temperature but this propensity holds also at high temperature, indicating that the cross-sections follow the energy gap law (at least for $\Delta j \leq 4$).

We have also checked the reliability of the rigid-rotor approximation for the CH$^+$ excitation by H. It was shown recently that this approximation leads to good results in the case of the endothermic OH$^+$+H reaction on the quartet PES whose minimum is similar to a van der Waals well (Bulut, Lique & Roncero 2015; Stoecklin et al. 2015). Its accuracy was found, however, to degrade on the doublet PES where there is a much deeper potential well, like in CH$^+$ + H (Bulut et al. 2015). We have performed rigid-rotor calculations with the TIQM code NEWMAT (Stoecklin, Voronin & Rayez 2003) combined with the CH_2^+ PES of Werfelli et al. (2015) where the CH$^+$ bond length was frozen at its equilibrium geometry. As shown in Fig. 3, the rigid-rotor approximation is found to be very inaccurate for CH$^+$+H. Indeed, although full-dimensional and rigid calculations have similar propensity rules, the cross-sections differ by up to 1 order of magnitude. In the full-dimensional treatment, the largest fraction of the scattering flux is thus directed into the reactive channel, as expected. This illustrates the importance of full-dimensionality for this reactive system. In the right-hand panel, we also compare the present rigid calculations with the rigid-rotor CH$^+$–He data of Turpin et al. (2010). Perhaps surprisingly, the agreement with the full-dimensional CH$^+$+H calculations is much better, in particular above 100 K. This fortuitous agreement is simply due to the much less attractive CH$^+$–He PES.

In Fig. 4, the rate coefficients for the exothermic destruction process CH$^+$(j)+H $\rightarrow$ C$^+$+H_2 are plotted as functions of the kinetic temperature and they are compared to the available measurements. As observed by Werfelli et al. (2015), the agreement between the calculated thermal rate coefficient and the experimental data (Federer et al. 1984, 1985; Luca, Borodi & Gerlich 2006; Plasil et al. 2011) is good above $T_k = 50$ K. In particular, the decrease of the rate coefficient between 400 and 1200 K is well reproduced by the calculations. At temperatures below 50 K, the experimental results at 12.2, 30 and 40 K were interpreted by Plasil et al. (2011) as a loss of reactivity of the lowest rotational states of CH$^+$. In contrast, we observe here a reactivity increase with rotational cooling. This was analysed by Werfelli et al. (2015) as an increase of the probability for a non-reactive or exchange process with increasing rotational excitation. Obviously, further theoretical and experimental efforts are necessary to understand this discrepancy at low temperature, as discussed in Plasil et al. (2011) and Werfelli et al. (2015).

2.3 Excitation and destruction by electrons

The calculations presented in this section are taken from Hamilton, Faure & Tennyson (2016) for the electron-impact excitation of CH$^+$ and from Epée Epée et al. (in preparation) for the dissociative recombination (DR) of CH$^+$ with electrons. In the calculations of Hamilton et al. (2016), the molecular **R**-matrix theory was

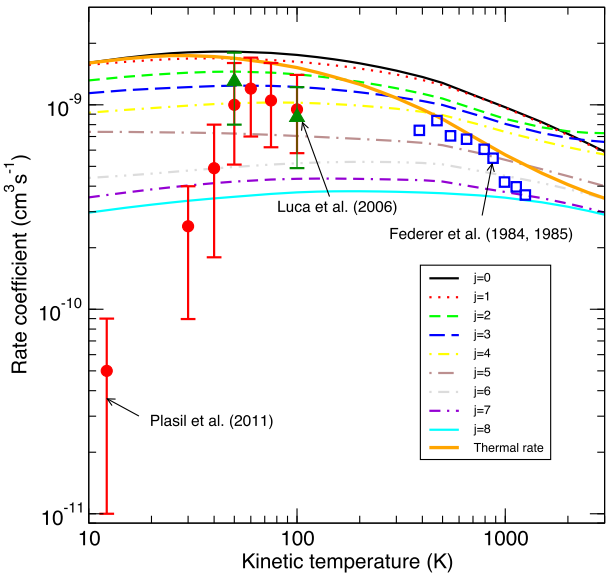

Figure 4. Rate coefficients for the destruction of $CH^+(j)$ by H as functions of the kinetic temperature. The initial-state-specific and thermal rate coefficients from this work are compared to the experimental data of Plasil et al. (2011), Luca et al. (2006) and Federer et al. (1984,1985).

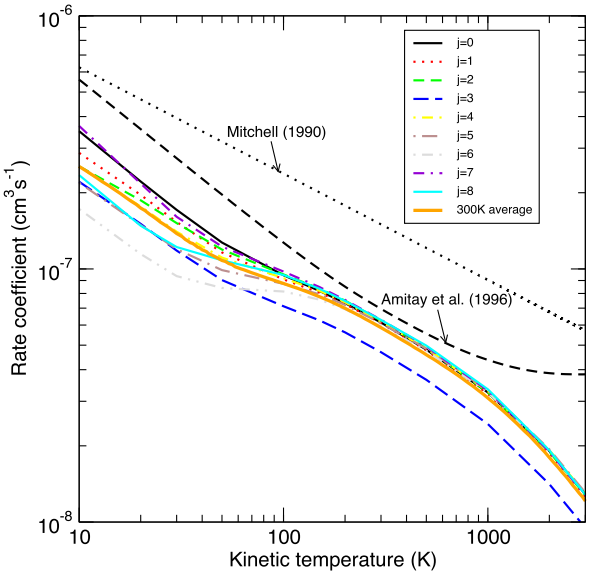

Figure 5. Rate coefficients for the destruction of $CH^+(j)$ by electrons as functions of the kinetic temperature. The initial-state-specific and 300 K thermal rate coefficients from this work are compared to the experimental results of Amitay et al. (1996) and Mitchell (1990).

combined with the adiabatic nuclei rotation (ANR) approximation. Inelastic cross-sections and rate coefficients were determined for $CH^+(j = 0–11)$ and kinetic temperatures in the range 1–3000 K. No experimental inelastic data are available for this system, but we note that the same methodology was applied with success to HD^+ for which theoretical rate coefficients were found comparable to within 30 per cent with those resulting from a fit of experimental cooling curves (Shafir et al. 2009). Very good agreement with the MQDT calculations of Motapon et al. (2014) for HD^+ and those of Epée Epée et al. (2016) for H_2^+ was also observed. In the calculations of Epée Epée et al. (in preparation), the MQDT formalism was employed: Based on the diabatic potential energy curves and the interaction between the ionization and the dissociation continua within the $^2\Pi$ symmetry used by Carata et al. (2000), we have computed the interaction, reaction and scattering matrices, and produced the DR cross-sections for the 11 lowest rotational levels of CH^+ in its ground electronic and vibrational state. Rate coefficients were determined for the DR of $CH^+(j = 0–10)$ at kinetic temperatures between 10 and 3000 K. The CH^+ thermal DR cross-section (after convolution with the experimental resolution) was found in satisfactory agreement with the measurements of Amitay et al. (1996) below 100 meV, and especially below 50 meV. Full details will be published elsewhere (Epée Epée et al., in preparation).

The rate coefficients for the inelastic process $CH^+(j = 0) + e^- \rightarrow CH^+(j')+ e^-$ are discussed in Hamilton et al. (2016) where full details can be found. In their fig. 3, the temperature dependences of the rate coefficients are found to be similar to those observed here for $CH^+ + H$ (Fig. 2) due to the threshold effects. Dipolar transitions $\Delta j = 1$ were found to be preferred, as expected for a strongly polar target. We note that this is in contrast with the previous **R**-matrix results of Lim et al. (1999), who found the cross-sections for the $\Delta j = 2$ transitions to be greater than $\Delta j = 1$ transitions. This difference was attributed by Hamilton et al. (2016) to the improved treatment of polarization in the new calculations.

In Fig. 5, the initial-state-specific DR rate coefficients are plotted as functions of the kinetic temperature. These rate coefficients were obtained by averaging the cross-sections over isotropic Maxwell-Boltzmann velocity distributions. The thermal average at a rotational temperature of 300 K is also shown and it is compared to two sets of experimental rate coefficients. The first was obtained from a thermal average of the DR cross-sections measured by Amitay et al. (1996), where the ions were assumed to be thermalized at the ambient temperature of the storage ring (300 K). The second is the experimental recommendation of Mitchell (1990). This later is based on the merged-beam data of Mitchell & McGowan (1978; divided by 2 to correct for a calibration error). The recommendation of Mitchell (1990) is found to exceed the results of Amitay et al. (1996) by about a factor of 2. The theoretical thermal average at 300 K is significantly lower but the agreement with Amitay et al. (1996) is within a factor of 2 up to ∼1000 K. It should be noted that the variation of the DR rate coefficients is not monotonic with j, i.e. there is no particular trend with increasing j. Such variations were already observed in the case of HD^+ (Motapon et al. 2014) and of H_2^+ (Epée Epée et al. 2016). In contrast to these systems, however, the rotational effects are weak in CH^+ and all initial-state-specific rates agree to within a factor of 2.

Finally, we note that all above collisional data are available upon request to the authors.

3 RADIATIVE TRANSFER MODEL

In order to illustrate the impact of the newly computed rate coefficients for the CH^+ formation, excitation and destruction, we now implement these data in a non-LTE radiative transfer model of CH^+ excitation in PDR conditions. PDRs are predominantly neutral regions of the ISM where the gas is exposed to FUV radiation fields (∼6–13.6 eV). PDRs typically occur at the boundaries of planetary nebulae, on the edges of molecular clouds and in the nuclei of starburst and active galaxies (Sternberg & Dalgarno 1995). A PDR thus starts at the fully ionized 'H II' region where only FUV radiation penetrates the neutral gas, i.e. stellar photons that cannot ionize hydrogen atoms but do ionize elements with low ionization potential (<13.6 eV) such as carbon. The C^+ column density thus

increases with the intensity of FUV radiation and it decreases with gas density. Inside the PDR, the FUV photon flux is indeed limited by H_2 and dust absorption. Beyond the edge of the C^+ zone, carbon is rapidly incorporated into CO. PDR models indicate that the CH^+ abundance peaks at visual extinctions $A_V \sim 0.1$–1 where the carbon is fully ionized and where the amount of vibrationally excited H_2 is high ($f^* = n(v_{H_2} > 0)/n(v_{H_2} = 0) > 10^{-6}$; Agúndez et al. 2010; Godard & Cernicharo 2013; Nagy et al. 2013). In this zone, hydrogen is predominantly in atomic form, most of the electrons are provided by the ionization of carbon atom, the kinetic temperature T_k is a few hundreds of Kelvin and the thermal pressure ($P/k_B = n_H T_k$) is about 10^8 K cm^{-3}. Obviously, the physical conditions in PDRs encompass a range of temperatures and densities with a rather complex morphology, as revealed recently with ALMA (Goicoechea et al. 2016). In the following, however, we will assume that CH^+ probes a region with homogeneous density and temperature, corresponding to the 'hot gas at average density' described by Nagy et al. (2017) for the Orion Bar.

As explained in the Introduction, since CH^+ is destroyed by hydrogen atoms and electrons on a similar time-scale as it is rotationally equilibrated (by the same colliders), the chemical formation and destruction rates need to be included when computing the statistical equilibrium equation (e.g. van der Tak et al. 2007):

$$\frac{dn_i}{dt} = \sum_{i\neq j}^{N} n_j P_{ji} - n_i \sum_{i\neq j}^{N} P_{ij} + F_i - n_i D_i = 0. \quad (2)$$

In this equation, N is the number of levels considered, n_i is the level population of level i, P_{ji} and P_{ij} are the populating and depopulating rates:

$$P_{ij} = \begin{cases} A_{ij} + B_{ij}\bar{J}_\nu + C_{ij} & (i > j) \\ B_{ij}\bar{J}_\nu + C_{ij} & (i < j), \end{cases} \quad (3)$$

and F_i and D_i are the state-resolved formation and destruction rates, respectively, of level n_i. In equation (3), $\bar{J}_\nu$ denotes the specific intensity integrated over line profile and solid angle, and averaged over all directions. The proportionality rates A_{ij} and B_{ij} are the Einstein coefficients for spontaneous and stimulated emission, respectively, and the C_{ij} are the collisional rates, i.e. the product of the collisional rate coefficients (in cm^3 s^{-1}) and the collider density (in cm^{-3}), summed over all possible collision partners (here H and e$^-$). Note that in equation (3), the notation $i > j$ means all states i with an energy higher than the energy of level j.

The main difficulty in solving the radiative transfer problem is the interdependence between the level populations and the local radiation field. Among approximate methods, the escape probability technique (e.g. Castor 1970) is widely employed. It is not adapted to model inhomogeneous sources, for which more sophisticated treatments are available (see e.g. Lambert et al. 2015, and references therein), but it is very useful in describing global average properties. In this work, we have employed the public version of the RADEX code[1] that uses the escape probability formulation assuming an isothermal and homogeneous medium. In its public version, the formation and destruction rates are assumed to be zero. We have therefore implemented in RADEX the inclusion of the source (F_i in cm^3 s^{-1}) and sink (D_i in s^{-1}) terms, which requires only minor modifications. It should be noted that only the relative values of F_i matter since the CH^+ column density is fixed within RADEX. As a result, the column densities of C^+ and $H_2(v_{H_2} > 0)$ are implicit

[1] http://home.strw.leidenuniv.nl/~moldata/radex.html

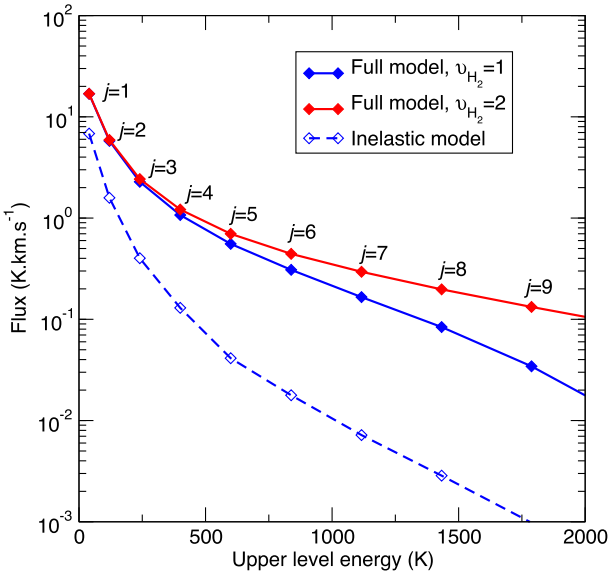

Figure 6. CH^+ line fluxes of $j \rightarrow j-1$ rotational transitions as functions of the upper level energy as predicted by our non-LTE calculations for the following PDR conditions: a pressure of 10^8 K cm^{-3} ($T_k = 500$ K, $n_H = 2 \times 10^5$ cm^{-3}), an electron fraction x_e of 10^{-4} and a CH^+ column density of 10^{14} cm^{-2}. See text for details on the three different models.

parameters in our calculations. The adopted formation rates correspond to H_2 in the inital state ($v_{H_2} = 1$, $j_{H_2} = 1$) or, alternatively, ($v_{H_2} = 2$, $j_{H_2} = 0$) (see below).

3.1 Prototypical PDR

The input parameters to RADEX are the kinetic temperature, T_k, the column density of CH^+, $N(CH^+)$, the line width, Δv, and the density of the colliding partners, n_H and $n(e^-)$. For a prototypical PDR, the thermal pressure is of the order of 10^8 K cm^{-3} (see above). Here, the density was set at $n_H = 2 \times 10^5$ cm^{-3} and the kinetic temperature at $T_k = 500$ K. We adopted a typical electron fraction of $x_e = n(e^-)/n_H = 10^{-4}$, as expected if carbon is fully ionized (for a standard ISM carbon elemental abundance). The line width was fixed at 5 kms^{-1} as observed in the Orion Bar (Nagy et al. 2013) and the CH^+ column density was set at 10^{14} cm^{-2}, corresponding to an average CH^+ abundance of $\sim 10^{-8}$. Finally, we assumed the cosmic microwave background (CMB) as the only background radiation field with a temperature of 2.73 K. It was indeed shown by Godard & Cernicharo (2013) that radiative pumping has only a minor influence on the CH^+ rotational distribution.

In Fig. 6, the line fluxes of the rotational series $j \rightarrow j-1$ from $j = 1 \rightarrow 0$ to $j = 9 \rightarrow 8$ are plotted as functions of the upper level energies for three different calculations: In the first, the public version of RADEX was employed, which entirely neglects the formation and destruction rates of CH^+. The rotational distribution of CH^+ is therefore established only through inelastic collisions with hydrogen atoms and free electrons. In the second calculation, the full model, which considers the formation of CH^+ *via* $C^+ + H_2(v_{H_2} = 1, j_{H_2} = 1)$ and its destruction *via* reactive collisions with hydrogen atoms and electrons, is employed. In the third calculation, the formation rates are those corresponding to $H_2(v_{H_2} = 2, j_{H2} = 0)$. The relative populations of the vibrationally excited states of H_2 are not known with precision but the state $v_{H_2} = 2$ can reach a population of $\sim 0.3 - 0.5$ with respect to the $v_{H_2} = 1$ state, e.g. in the Orion Bar (van der Werf et al. 1996;

Walmsley et al. 2000). The $v_{H_2} = 2$ state can therefore play an important role in the chemical pumping of CH^+. We can first observe in Fig. 6 that the inclusion of formation and destruction rates ('full model') increases the fluxes of the lines by at least a factor of 2 and up to 2 orders of magnitude. This clearly illustrates the importance of chemical pumping, even for the lowest $j = 1 \rightarrow 0$ transition. The impact of the $v_{H_2} = 2$ state is to further increase the line fluxes, especially for transitions above $j = 4$. This is easily explained by looking at the rotational distributions of the nascent $CH^+(v = 0, j)$ in Fig. 1: The probability for $v_{H_2} = 2$ peaks at higher j than $v_{H_2} = 1$ and this initial hotter distribution translates into a larger final excitation. This demonstrates that the memory of the CH^+ formation process is transferred to, and preserved in the rotational distribution. In other words, the radiative cascade subsequent to the initial formation of CH^+ is dominant over the pure inelastic (excitation and de-excitation) processes.

3.2 The Orion Bar

The Orion Bar PDR is the archetypal edge-on molecular cloud surface illuminated by FUV radiation from nearby massive stars. The presence of vibrationally excited H_2 in this source is supported by infrared observations of the $v_{H_2} = 1 \rightarrow 0$ and $v_{H_2} = 2 \rightarrow 1$ transitions (van der Werf et al. 1996). CH^+ was first detected in the Orion Bar by Naylor et al. (2010) and Habart et al. (2010), based on *Herschel*-SPIRE maps of the $j = 1 \rightarrow 0$ transition. These studies were then extended, thanks to *Herschel*-HIFI and *Herschel*-PACS data with the detection of the full rotational series up to $j = 6 \rightarrow 5$ by Nagy et al. (2013). Recently, the spatial distribution of CH^+ was found to be well correlated with that of the $v_{H_2} = 1 \rightarrow 0$ line of H_2 in this source (Parikka et al. 2017), as predicted by Agúndez et al. (2010). Previous non-LTE models including chemical pumping for the Orion Bar can be found in Godard & Cernicharo (2013), Zanchet et al. (2013) and Nagy et al. (2013).

In our non-LTE calculations, we adopted the same physical conditions as for the above prototypical PDR, except that the CH^+ column density is a free parameter adjusted to best reproduce the observations of Nagy et al. (2013), assuming a unit filling factor.[2] Very good agreement is observed in Fig. 7 between the model ($v_{H_2} = 1$) and the observations for a CH^+ column density of 9×10^{13} cm^{-2}, corresponding to a column density per unit line width of 1.8×10^{13} cm^{-2}(km s^{-1})$^{-1}$. Indeed, the calculations agree within error bars with *Herschel* data, except for the highest transition. This column density is in excellent agreement with that derived by Morris et al. (2016) for the Orion BN/KL average. It is however a factor of 10 lower than the value of Nagy et al. (2013) for the Orion Bar. These authors have employed similar physical conditions but lower densities and different collisional and chemical rates, which likely explains the differences and illustrates the importance of accurate microphysics data. In Fig. 7, we have also reported our results when the formation rates are those for $H_2(v_{H_2} = 2, j_{H2} = 0)$. As expected, these rates produce a hotter rotational distribution (see also Fig. 6) and the flux of the lines $j = 5 \rightarrow 4$ and $j = 6 \rightarrow 5$ is higher than that observed, suggesting that the relative population of $v_{H_2} = 2$ is not large in the Orion Bar. We note, finally, that the contribution of electron collisions is small at an electron fraction

[2] We note that the flux of the two *Herschel*-HIFI lines reported in table 2 of Nagy et al. (2013) were corrected for main beam efficiencies (Nagy Z., private communication).

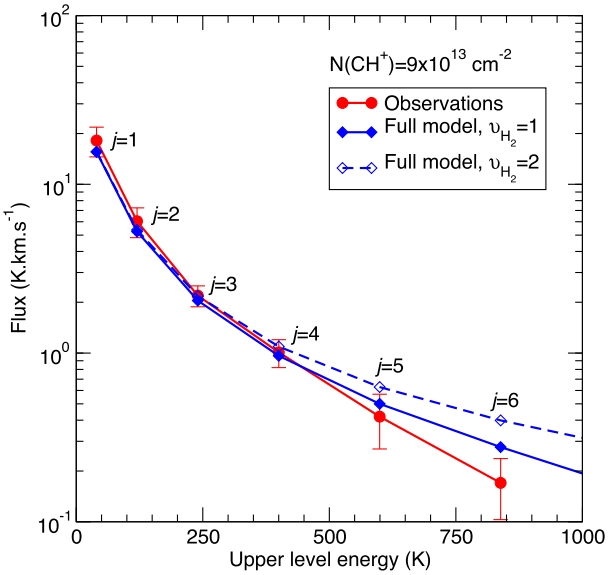

Figure 7. Same as in Fig. 6 except that the CH^+ column density is adjusted to best reproduce the observations of Nagy et al. (2013) towards the Orion Bar.

$x_e = 10^{-4}$: The largest effect is a 11 per cent increase in the intensity of the ground-state $j = 1 \rightarrow 0$ transition, as observed by Nagy et al. (2013). The excitation and destruction of CH^+ in this source is therefore dominated by hydrogen collisions.

3.3 NGC 7027

NGC 7027 is a prototypical young planetary nebula in which the circumstellar gas is exposed to a high FUV flux emanating from the hot central white dwarf. A large fraction of vibrationally excited H_2 ($f^* \sim 10^{-3}$) is predicted for this source (Agúndez et al. 2010). The presence of excited H_2 was established by *ISO* observations of several $v_{H_2} = 1 \rightarrow 0$ transitions (Bernard Salas et al. 2001). CH^+ was discovered in this source by Cernicharo et al. (1997) with the *ISO* detection of five rotational lines from $j = 2 \rightarrow 1$ to $j = 6 \rightarrow 5$. The ground-state line $j = 1 \rightarrow 0$ was detected more recently with *Herschel*-SPIRE by Wesson et al. (2010). These authors have shown that the six rotational lines cannot be fitted by a single excitation temperature. The first non-LTE model including chemical pumping for NGC 7027 was presented by Godard & Cernicharo (2013).

In our non-LTE calculations, we adopted the same hydrogen density and kinetic temperature as for the above prototypical PDR but the other parameters were modified as follows: The electron fraction was increased to $x_e = 10^{-3}$ to account for the higher elemental carbon abundance in this carbon rich circumstellar envelope (Godard & Cernicharo 2013), and the line width was set at 30 km s^{-1}, as in Cernicharo et al. (1997). We also assumed that the size of the CH^+ emission in the PDR is 10 arcsec (Cox et al. 2002). Finally, the CH^+ column density is again the free parameter adjusted to best reproduce the *ISO* and *Herschel* observations. Note that the flux towards NGC 7027 was measured in W cm^{-2} (not in K km s^{-1}) so that it does not decline monotically with increasing upper level energy. Good agreement is observed in Fig. 8 between the model and the observations, although the fluxes of the highest transitions $j = 5 \rightarrow 4$ and $j = 6 \rightarrow 5$ are underproduced when H_2 is initially in $v_{H_2} = 1$. The best model is obtained for a large CH^+ column density of 2×10^{15} cm^{-2}, corresponding to a column density per unit line width of 6.7×10^{13} cm^{-2}(km s^{-1})$^{-1}$, in good agreement with

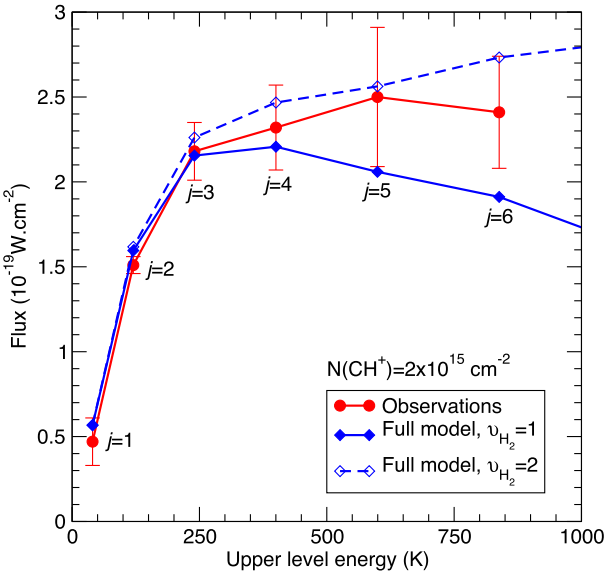

Figure 8. Same as in Fig. 6 except that the electron fraction is $x_e = 10^{-3}$ and the CH$^+$ column density is adjusted to best reproduce the observations of Cernicharo et al. (1997) and Wesson al. (2010) towards NGC 7027.

Godard & Cernicharo (2013). Fig. 8 also reports our results when the formation rates are those for $H_2(\nu_{H_2} = 2, j_{H2} = 0)$. The agreement with *ISO* observations is now within error bars. This suggests that the relative population of the state $\nu_{H_2} = 2$ could be large in the PDR of NGC 7027. The observations of higher frequency transitions of CH$^+$ ($j = 7 \rightarrow 6$, etc.) might help to confirm this result. Finally, we note that the contribution of electron collisions is substantial here at an electron fraction $x_e = 10^{-3}$ cm^{-3}: A 75 per cent increase in the intensity of the ground-state $j = 1 \rightarrow 0$ transition was observed. This effect decreases for higher transitions but electrons still contribute above 10 per cent for the $j = 4 \rightarrow 3$ transition. As a result, electrons compete with hydrogen atoms for the excitation and destruction of CH$^+$ in this carbon-rich circumstellar envelope.

4 CONCLUSION

We have presented a detailed theoretical study of the rotational excitation of CH$^+$ due to chemical pumping, excitation and destruction. The investigated colliders were hydrogen atoms and free electrons. State-to-state and initial-state-specific rate coefficients were computed for the inelastic, exchange, abstraction and dissociative recombination processes using the best available PESs and scattering methods. State-to-state rate coefficients were also computed for the formation reaction, $C^+(^2P)+H_2(\nu_{H_2}, j_{H_2}) \rightarrow CH^+ + H$, by extending the calculations of Zanchet et al. (2013) to the vibrationally excited state ($\nu_{H_2} = 2$, $j_{H_2} = 0$). Good agreement with available experimental thermal rate coefficients was observed, except for the abstraction reaction CH$^+$+H at low temperature (<50 K). The full set of collisional and chemical data were then implemented in a radiative transfer model based on the escape probability formalism. These non-LTE calculations have confirmed previous studies that suggested that chemical pumping has a substantial effect on the excitation of CH$^+$ in PDRs (Godard & Cernicharo 2013; Nagy et al. 2013; Zanchet et al. 2013). However, in contrast to these previous works, we have employed for the first time a comprehensive theoretical set of fully state-to-state data. Our non-LTE model was applied to typical PDR conditions and, in particular, to two prototypical sources: the Orion Bar and the planetary nebula NGC 7027. We were able to reproduce, within error bars, the *ISO* and *Herschel* measurements by adjusting the CH$^+$ column density as a single free parameter.

Obviously, there is no unique solution and this work can be further improved e.g. by computing self-consistently the CH$^+$ abundance, instead of fixing its column density. The impact of the H_2 rotational distribution within the different vibrational manifolds should be also investigated. This will require to extend the calculations on $C^+(^2P)+H_2(\nu_{H_2}, j_{H_2})$ to higher rotational levels $j_{H_2} > 1$, of particular importance in the ground vibrational state $\nu_{H_2} = 0$. Collisions between CH$^+$ and H_2 should be also considered. We have assumed in this work that hydrogen is in atomic form in the region of maximum CH$^+$ abundance. However, a non-negligible molecular hydrogen fraction is necessary to form CH$^+$ from $C^+ + H_2$. The knowledge of state-to-state rate coefficients for the $CH^+ + H_2$ collisions might even provide constraints to the H_2 fraction. Calculations of the PES for the electronic ground state of CH_3^+ are in progress in Bordeaux (Halvick and co-workers). Finally, the generalization of this work to the excitation of other reactive species such as OH$^+$ and SH$^+$, for which state-resolved formation rates are becoming available (Gómez-Carrasco et al. 2014; Zanchet, Roncero & Bulut 2016), will be presented in future works.

ACKNOWLEDGEMENTS

This work has been supported by the Agence Nationale de la Recherche (ANR-HYDRIDES), contract ANR-12-BS05-0011-01 and by the CNRS national programme 'Physico-Chimie du Milieu Interstellaire'. IFS acknowledges generous financial support from Région Haute-Normandie, the GRR Electronique, Energie et Matériaux, the 'Fédération de Recherche Energie, Propulsion, Environnement', the fund Bioengine and the LabEx EMC, via the project PicoLIBS. OR and AZ acknowledge the financial support of Ministerio de Economia e Innovación under grant FIS2014-52172-C2 and the European Research Council under ERC Grant Agreement n. 610256 (NANOCOSMOS). François Lique and Pierre Hily-Blant are acknowledged for useful discussions.

REFERENCES

Agúndez M., Goicoechea J. R., Cernicharo J., Faure A., Roueff E., 2010, ApJ, 713, 662
Amitay Z. et al., 1996, Phys. Rev. A, 54, 4032
Bakker E. J., van Dishoeck E. F., Waters L. B. F. M., Schoenmaker T., 1997, A&A, 323, 469
Bernard Salas J., Pottasch S. R., Beintema D. A., Wesselius P. R., 2001, A&A, 367, 949
Black J. H., 1998, Faraday Discussions, 109, 257
Bonnet L., 2013, Int. Rev. Phys. Chem., 32, 171
Bovino S., Grassi T., Gianturco F. A., 2015, J. Phys. Chem. A, 119, 11973
Bulut N., Lique F., Roncero O., 2015, J. Phys. Chem. A, 119, 12082
Carata L., Orel A. E., Raoult M., Schneider I. F., Suzor-Weiner A., 2000, Phys. Rev. A, 62, 052711
Castor J. I., 1970, MNRAS, 149, 111
Cernicharo J., Liu X.-W., González-Alfonso E., Cox P., Barlow M. J., Lim T., Swinyard B. M., 1997, ApJ, 483, L65
Cox P., Huggins P. J., Maillard J.-P., Habart E., Morisset C., Bachiller R., Forveille T., 2002, A&A, 384, 603
Douglas A. E., Herzberg G., 1941, ApJ, 94, 381
Epée Epée M. D., Mezei J. Z., Motapon O., Pop N., Schneider I. F., 2016, MNRAS, 455, 276
Falgarone E. et al., 2010, A&A, 518, L118

Federer W., Villinger H., Howorka F., Lindinger W., Tosis P., Bassi D., Ferguson E., 1984, Phys. Rev. Lett., 52, 2084
Federer W., Villinger H., Tosi P., Bassi D., Ferguson E., Lindinger W., 1985, in Diercksen G. H. F., Huebner W. F., Langhoff P. W., eds, Molecular Astrophysics, NATO Advanced Science Institutes (ASI) Series C, Vol. 157. Reidel, Dordrecht, p. 649
Gerlich D., Disch R., Scherbarth S., 1987, J. Chem. Phys., 87, 350
Godard B., Cernicharo J., 2013, A&A, 550, A8
Godard B., Falgarone E., Pineau des Forêts G., 2014, A&A, 570, A27
Goicoechea J. R. et al., 2016, Nature, 537, 207
Gómez-Carrasco S. et al., 2014, ApJ, 794, 33
Grozdanov T. P., McCarroll R., 2013, Chem. Phys. Lett., 575, 23
Habart E. et al., 2010, A&A, 518, L116
Hamilton J. R., Faure A., Tennyson J., 2016, MNRAS, 455, 3281
Hammami K., Owono Owono L. C., Stäuber P., 2009, A&A, 507, 1083
Herráez-Aguilar D., Jambrina P. G., Menéndez M., Aldegunde J., Warmbier R., Aoiz F. J., 2014, Phys. Chem. Chem. Phys., 16, 24800
Hierl P. M., Morris R. A., Viggiano A. A., 1997, J. Chem. Phys., 106, 10145
Lambert J., Josselin E., Ryde N., Faure A., 2015, A&A, 580, A50
Li Y. Q., Zhang P. Y., Han K. L., 2015, J. Chem. Phys., 142, 124302
Lim A. J., Rabadán I., Tennyson J., 1999, MNRAS, 306, 473
Luca A., Borodi G., Gerlich D., 2006, in Fainstein P. D., Lima M. A. P., Miraglia J. E., Montenegro E. C., Rivarola R. D., eds, Photonic, Electronic and Atomic Collisions. World Scientific Publishing Co. Pvt. Ltd., Singapore, p. 494
Mitchell J. B. A., 1990, Phys. Rep., 186, 215
Mitchell J. B. A., McGowan J. W., 1978, ApJ, 222, L77
Morris P. W. et al., 2016, ApJ, 829, 15
Motapon O. et al., 2014, Phys. Rev. A, 90, 012706
Nagy Z. et al., 2013, A&A, 550, A96
Nagy Z. et al., 2017, A&A, 599, A22
Naylor D. A. et al., 2010, A&A, 518, L117
Oka T., Welty D. E., Johnson S., York D. G., Dahlstrom J., Hobbs L. M., 2013, ApJ, 773, 42
Parikka A. et al., 2017, A&A, 599, A20
Plasil R., Mehner T., Dohnal P., Kotrik T., Glosik J., Gerlich D., 2011, ApJ, 737, 60
Shafir D. et al., 2009, Phys. Rev. Lett., 102, 223202
Skouteris D., Castillo J. F., Manolopoulos D. E., 2000, Comput. Phys. Commun., 133, 128
Sternberg A., Dalgarno A., 1995, ApJS, 99, 565
Stoecklin T., Halvick P., 2005, Phys. Chem. Chem. Phys., 7, 2446
Stoecklin T., Voronin A., Rayez J. C., 2003, Phys. Rev. A, 68, 032716
Stoecklin T., Gannouni M. A., Jaidane N. E., Halvick P., Hochlaf M., 2015, J. Phys. Chem. A, 119, 12599
Thi W.-F. et al., 2011, A&A, 530, L2
Turpin F., Stoecklin T., Voronin A., 2010, A&A, 511, A28
van der Tak F. F. S., Black J. H., Schöier F. L., Jansen D. J., van Dishoeck E. F., 2007, A&A, 468, 627
van der Werf P. P., Stutzki J., Sternberg A., Krabbe A., 1996, A&A, 313, 633
van der Werf P. P. et al., 2010, A&A, 518, L42
Walmsley C. M., Natta A., Oliva E., Testi L., 2000, A&A, 364, 301
Warmbier R., Schneider R., 2011, Phys. Chem. Chem. Phys., 13, 10285
Werfelli G., Halvick P., Honvault P., Kerkeni B., Stoecklin T., 2015, J. Chem. Phys., 143, 114304
Wesson R. et al., 2010, A&A, 518, L144
Zanchet A., Godard B., Bulut N., Roncero O., Halvick P., Cernicharo J., 2013, ApJ, 766, 80
Zanchet A., Roncero O., Bulut N., 2016, Phys. Chem. Chem. Phys., 18, 11391

This paper has been typeset from a TEX/LATEX file prepared by the author.